



Spatial and seasonal patterns of rainfall erosivity in the Lake Kivu region: Insights from a meteorological observatory network

R.M. Bagalwa

Université Catholique de Louvain, Belgium
Observatoire Volcanologique de Goma, DR Congo

C. Chartin

Université Catholique de Louvain, Belgium

S. Baumgartner 

Université Catholique de Louvain, Belgium
Ghent University, Belgium

S. Mercier

Université Catholique de Louvain, Belgium

M. Syauswa

Observatoire Volcanologique de Goma, DR Congo

V.C. Samba

Observatoire Volcanologique de Goma, DR Congo

M.T. Zabona

Observatoire Volcanologique de Goma, DR Congo

K. Karume

Observatoire Volcanologique de Goma, DR Congo
Université Evangélique en Afrique, Bukavu, DR Congo

N.L. Cizungu

Université Catholique de Bukavu, DR Congo

M. Barthel

Swiss Federal Institute of Technology, ETH Zürich, Switzerland

S. Doetterl

Swiss Federal Institute of Technology, ETH Zürich, Switzerland

J. Six

Swiss Federal Institute of Technology, ETH Zürich, Switzerland

P. Boeckx

Ghent University, Belgium

K. Van Oost

Université Catholique de Louvain, Belgium

Abstract

In the Lake Kivu region, water erosion is the main driver for soil degradation, but observational data to quantify the extent and to assess the spatial-temporal dynamics of the controlling factors are hardly available. In particular, high spatial and temporal resolution rainfall data are essential as precipitation is the driving force of soil erosion. In this study, we evaluated to what extent high temporal resolution data from the TAHMO network (with poor spatial and long-term coverage) can be combined with low temporal resolution data

Corresponding author:

Simon Baumgartner, Université Catholique de Louvain, UCL, Louvain-la-Neuve, 1348, Belgium.

Email: simon.baumgartner@uclouvain.be

(with a high spatial density covering long periods of time) to improve rainfall erosivity assessments. To this end, 5 minute rainfall data from TAHMO stations in the Lake Kivu region, representing ca. 37 observation-years, were analyzed. The analysis of the TAHMO data showed that rainfall erosivity was mainly controlled by rainfall amount and elevation and that this relation was different for the dry and wet season. By combining high and low temporal resolution databases and a set of spatial covariates, an environmental regression approach (GAM) was used to assess the spatiotemporal patterns of rainfall erosivity for the whole region. A validation procedure showed relatively good predictions for most months (R^2 between 0.50 and 0.80), while the model was less performant for the wettest (April) and two driest months (July and August) (R^2 between 0.24 and 0.38). The predicted annual erosivity was highly variable with a range between 2000 and 9000 MJ mm ha⁻¹ h⁻¹ yr⁻¹ and showed a pronounced east–west gradient which is strongly influenced by local topography. This study showed that the combination of high and low temporal resolution rainfall data and spatial prediction models can be used to improve the assessments of monthly and annual rainfall erosivity patterns that are grounded in locally calibrated and validated data.

Keywords

Rainfall, erosivity, Lake Kivu, NLS, GAM

1 Introduction

In the Lake Kivu region (LKR), the larger cross-border region between the DR Congo, Rwanda, Uganda and Burundi, soil conservation faces challenges stemming from landslides and flooding, population growth, and limited access to resources, as well as a limited regulatory framework to impose prevention. With an average density of 160 inhabitants per square kilometer (Courtois and Manirakiza, 2015), the LKR is among the most densely populated areas of the African continent, relying largely on subsistence farming for food production and charcoal for energy. The increasing demand for food and energy puts large pressure on physical land resources in the region inducing land degradation. Soil loss by water erosion is one of the most important land degradation processes in the LKR (Karagame et al., 2016), but it is challenging to quantify its extent and impact. Limited local field observations make it difficult to gain a precise understanding and quantification of the phenomenon for the wider region (Vrieling et al., 2010). Achieving a thorough quantification of the spatiotemporal patterns of soil loss and their underlying drivers in the region, as well as the application of tools to predict

changes in soil loss, response to land management and climate change are paramount.

In a landscape with a steep topography, such as the LKR, precipitation is the driving force of soil erosion, and knowledge on rainfall erosivity is useful to contextualize the soil loss problem. The total kinetic energy of the rain exerted on the soil surface controls how much soil is being detached, while the amount of rainfall is an important control on transport of eroded materials. Rainfall erosivity is therefore typically described as the product of rainfall energy and maximum 30-minute intensity, such as in the R -factor (MJ mm ha⁻¹ h⁻¹ yr⁻¹) of the RUSLE (Wischmeier and Smith, 1978) and its predecessor the USLE (Wischmeier and Smith, 1958). It is well established that a few erosive events can contribute to a significant share of erosion (Vantas et al., 2019). However, long-term dense time series, i.e. with 5- to 30-minute logging intervals, from pluviographs are required to accurately estimate rainfall erosivity. These data are not always available, particularly in tropical Africa. Therefore, models have been developed that correlate rainfall erosivity with more readily available data (such as daily, monthly and annual precipitation amounts) to estimate

rainfall erosivity (e.g. Bonilla and Vidal, 2011; Vantas et al., 2019). For Africa, parametric equations relating R -factor estimates to the monthly values of rainfall depth have been developed for North Africa (Smithen and Schulze, 1982), Morocco (Arnoldus, 1977), Nigeria (Igwe et al., 1999) and Sudan (Elagib, 2011). Other studies have used parametric equations for the estimation of daily R -values based on daily rainfall depths. Those equations were developed for Kenya (Angima et al., 2003), Nigeria (Salako, 2010) and North Africa (Le Roux et al., 2008). For West Africa, Roose (1977) developed a simple linear relation between the yearly R -factors and rainfall, while Arnoldus (1977) used the modified Fournier index to estimate rainfall erosivity in Morocco. However, in general, these empirical equations provide only a rough indication of rainfall erosivity, and they cannot be applied outside the region of calibration without considerable uncertainty (e.g. Verstraeten et al., 2006). Furthermore, rainfall erosivity is typically characterized by a large inter- and intra-annual variability, and a representative R -factor therefore requires evaluation over a longer period (Renard and Freimund, 1994; Wischmeier and Smith, 1978). Reliable estimates of rainfall erosivity not only require high temporal resolution gauges recording but also good spatial coverage to assess its spatial variability. This is particularly relevant for the LKR, as the region is marked by a highly variable topography, with an elevation range between ca. 500 and 5000 m, active volcanoes and large low-land plains located within the inter-tropical convergence zone (ITCZ) resulting in strong rainfall seasonality with a large regional variability (Figure 1).

The availability of rain gauges that operate at high temporal resolution as part of a dense spatial network is an issue in tropical Africa. A recent literature review showed that less than 30 reliable weather stations reporting high-resolution rainfall data are available for the African continent as a whole (Ballesteros

et al., 2018; Panagos et al., 2017). A gray literature study by Ryumugabe and Berding (1992) is, to the best of our knowledge, the only assessment of rainfall erosivity that is based on local high-resolution rainfall data for the LKR. High-resolution data for the LKR covering more than a decade are available for only six stations (Ryumugabe and Berding, 1992; Rutebuka et al., 2020). However, stations in the study are all clustered in Rwanda at relatively low altitudes, and the underlying factors controlling variability in rainfall erosivity have not been quantified so far. Hence, data is also lacking for a large part of the LKR, including large and densely populated parts of the region (i.e. DR Congo, Burundi and Uganda).

Until now, studies have relied on relationships developed elsewhere (e.g. Lo et al., 1985) using coarse temporal scale data (monthly or even annual) (e.g. Muhire et al., 2015). Other approaches, based on remote-sensing or on continental-scale spatial models, have been proposed to improve erosivity assessments for Africa and have estimated the spatial patterns of erosivity in the Kivu region. These studies have shown that satellite-derived rainfall products typically do not represent high-intensity erosive events, but may, at least to some extent, represent the spatial variability of long-term average annual rainfall erosivity (Vrieling et al., 2010). However, these coarse-scale approaches are associated with considerable uncertainty at the local scale due to the lack of high temporal-resolution data for model calibration and evaluation.

Therefore, spatial and temporal patterns of rainfall erosivity in the LKR and tropical Africa in general are not well understood and poorly documented. However, there are some developments to help close crucial data gaps. In recent years, high-quality data collection efforts are being conducted across Africa for climate monitoring (TAHMO: Trans-African HydroMeteorological Observatory; www.tahmo.org). A dense network of meteorological

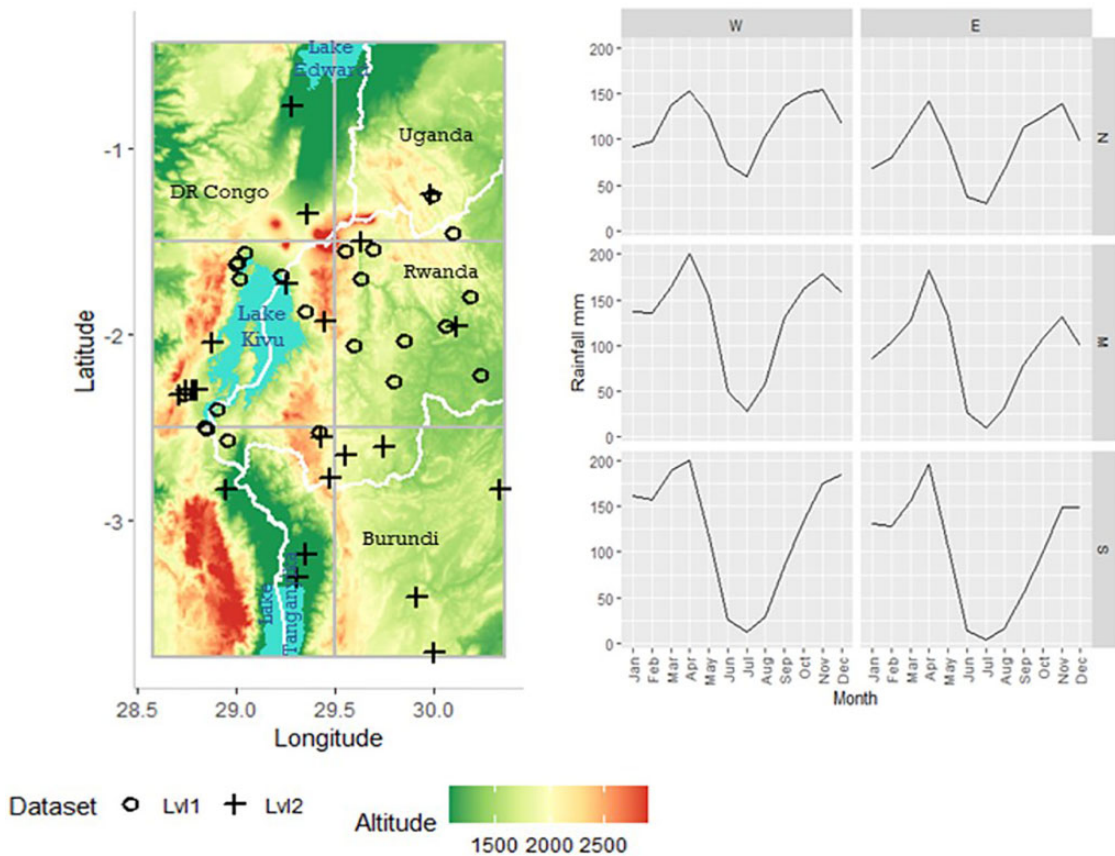


Figure 1. General topography and pluviometry of the study area with locations of the Lvl I and Lvl2 meteorological stations (see text for explanation). Note that for visualization purposes, two Lvl2 sites are outside the area shown. The panel on the right represents the long-term average rainfall patterns (1970–2000) for six sub-regions (indicated in gray boxes on the left panel). The rainfall data is derived from the WorldClim data base (Fick and Hijmans, 2017). The white lines represent national borders. N, S, W and E indicate wind directions, while M represents ‘middle or central area’.

stations has been installed since 2017 across Africa with the objective to have 20,000 operational stations. This type of effort has substantially increased the spatial coverage of high temporal resolution rainfall data across Africa but, so far, the potential of these data-sources for erosivity assessments has remained unexplored. Nevertheless, estimates of rainfall erosivity grounded in local observations are key to increase the confidence in rainfall and runoff erosivity as well as soil erosion assessments. Although the TAHMO network provides data

for 20 stations in the LKR, the short observation period (max. 3 years) does not allow constructing reliable spatiotemporal models of rainfall erosivity. However, low temporal resolution rainfall data at the monthly timescale is available for 24 stations in the LKR covering the period 1970–2000 (e.g. FAO Climwat database; CROPWAT Software, FAO, 2018). Although this dataset has an excellent spatial coverage in the LKR, its low temporal resolution does not allow it to be used directly for rainfall erosivity estimations.

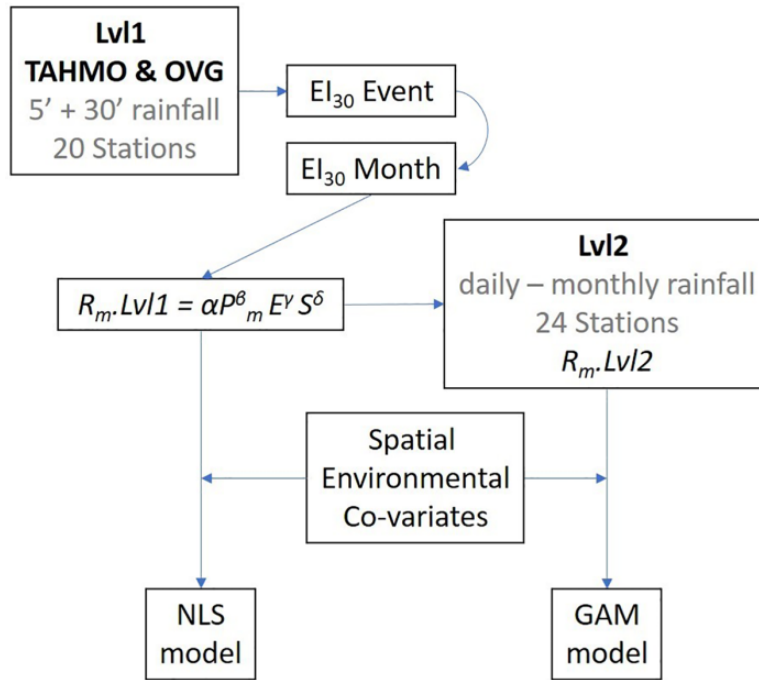


Figure 2. Flowchart of the methods used for this study.

The objective of this study is therefore to evaluate to what extent recent high temporal resolution data (but with poor spatial and long-term coverage) can be combined with low temporal resolution (but high spatial density covering long periods of time) data to improve rainfall erosivity assessments. To this aim, we: (a) analyze the factors controlling rainfall erosivity in the LKR based on new high temporal resolution data from the TAHMO network; (b) develop geostatistical models, which combine low- and high-resolution data to quantify the spatiotemporal patterns of both monthly and annual rainfall erosivity in the LKR; and (c) confront these new estimates, grounded in local observations, with existing estimates.

II Materials and methods

2.1 Study area

The Lake Kivu region is located in the highest part of the Albertine Rift and covers an area of

ca. 180,000 km² in Central–East Africa (Figure 1). The lowlands, lying between 1000 and 1500 m, receive rainfall of between 1000 and 1200 mm yr⁻¹ (Muhire et al., 2015; Ndayirukiye and Sabushimike, 2015). With altitudes ranging between 2000 and 3500 m, the highland region, which includes the Congo–Nile ridge and volcanic chains of Virunga, has a mean annual rainfall of 1300 to 1550 mm (Ilunga et al., 2004; Karagame et al., 2016). As illustrated in Figure 1, the meridional translation of the ITCZ leads to a bimodal distribution of the annual precipitation cycle over much of the region. The regions located in the most southerly parts of the study area are further away from the equator and at the limit of the extent of the ITCZ migration, resulting in a unimodal cycle of rainfall, with a dry period during boreal summer. This defines a latitudinal gradient in rainfall where the southern part receives more rain but has a more pronounced dry period (Figure 1).

2.2 Precipitation data

A flowchart of the data and approaches used is presented in Figure 2. Precipitation data at high temporal resolution (5-minute intervals), covering September 2017 to March 2020, were obtained from the TAHMO network for 20 stations available around Lake Kivu (5 in the DR Congo, 1 in Uganda and 14 in Rwanda) using the TAHMO web API (Figure 1). The TAHMO network uses ‘ATMOS 41 All-in-one’ weather stations (Meter Environment, Pullman, USA) and measures precipitation with a resolution of 0.017 mm and an accuracy of ca. 5%. Rainfall measurement is based on an acoustic disdrometer. Note that stations have been installed at different dates and therefore do not cover the same time period. We added another high-resolution dataset, the Goma Volcano Observatory (OVG) meteorological database, with continuous 30-minute interval data from one station in Goma (DRC) for the period 2012–2017 to the database. The different time resolutions (5 minutes vs 30 minutes) are explicitly addressed in Section 3.2. Together this database (called Lvl1) contains a total of 445 station-months, representing ca. 37 observation-years from 20 different stations. However, due to battery issues or internet connection problems, there are data gaps. To address this, we only considered observations from months where data were recorded more than 95% of the time. The observation months are equally distributed over the year, and the Lvl1 stations cover an elevation range that spans between 1352 and 2424 m.

Secondly, low temporal resolution data (daily to monthly), but covering several years to decades and having a good spatial coverage of the LKR, were gathered from different sources. This dataset is called Lvl2. First, we selected the 18 meteorological stations that were available for the LKR from the FAO CLIMWAT 2.0 for CROPWAT meteorological database (Table S1). The database presents

long-term average monthly rainfall for the period 1970–2000. In a second step, we added data from five stations extracted from the Rwanda meteorological database from the Rwandan Meteorological Center based in Kigali and the LWIRO meteorological database from Lwiro Meteorological Station based at LWIRO-C.R.S.N. The daily data for LWIRO and the Rwanda meteorological databases were aggregated to monthly observations and long-term monthly averages. In total, the Lvl2 dataset has 24 stations with long-term monthly rainfall data for the period 1970–2010. Details are provided in Table S1.

2.3 Erosivity calculations

To calculate the erosion index (EI) for a given rainfall event in the Lvl1 database we used the Rainfall Intensity Summarization Tool (RIST) software (USDA, 2019). In this method, the erosion index is calculated as a product of the kinetic energy of an event (E) and its maximum rainfall intensity over 30 minutes (I_{30}) for a period of 30 minutes (Renard and Freimund, 1994):

$$EI_{30} = \left(\sum_{r=1}^0 e_r v_r \right) I_{30} \quad (\text{Eq.1})$$

Where e_r represents rainfall energy per unit depth of rainfall in $\text{MJ ha}^{-1} \text{mm}^{-1}$, v_r is the volume of rainfall (mm) during a given time interval (r) and I_{30} is the maximum rainfall intensity over a 30-minute period of the rainfall event (mm h^{-1}). In an assessment of rainfall events in Rwanda, Rutebuka et al. (2020) showed that rainfall events with less than 8 mm cumulative rainfall experienced limited soil losses and identified these events as non-erosive; thus we did not include events with less than 8 mm cumulative rainfall in the estimation of monthly erosivity. Storm events were broken up when there was less than 1.27 mm rainfall in a 6-h period (Renard and Freimund, 1994). Rain energy per unit depth of rain for each increment

(e_r) ($\text{MJ ha}^{-1} \text{ mm}^{-1}$) is often calculated using relation that was developed by Brown and Foster (1987):

$$e_r = 0.29[1 - 0.72^{-0.05i_r}] \quad (\text{Eq.2})$$

This empirical equation was originally developed for the United States. We evaluated the representativeness of this equation for the LKR by analyzing published raindrop size distribution data from Butare, Rwanda (Adetan and Afullo, 2014). For six rainfall events with intensities ranging between 1 and 79 mm h^{-1} , we obtained a relative difference of only 13% between the observed rainfall energy and equation (2). This suggests that equation (2) can be reliably used to approximate rainfall energy also for the tropical conditions in the LKR. Monthly ($R_m\text{.Lv11}$) erosivity factors were then calculated by summing the EI_{30} values for each month.

The calculation of the maximum rainfall intensity during an erosive rainfall event (equation (1)) is influenced by the recording interval, and coarser intervals will lead to lower values. We evaluated how coarser measurement intervals (10, 30 and 60 minutes) affect the estimation of the rainfall erosivity by aggregating the 5-minute interval data to coarser temporal resolutions (Figure S1).

To analyze the factors controlling rainfall erosivity, we used regression models with $R_m\text{.Lv11}$ as the target variable. We explored the use of rate modifiers for elevation and season in equation (3) to represent the effect of environmental co-variables. We used a nonlinear regression to estimate the monthly erosivity. A similar approach has been used before to predict $R_m\text{.Lv11}$ (McGregor et al., 1995). Here we add two modifiers that represent topography and seasonality:

$$R_m\text{.Lv11} = \alpha P_m^\beta E^\gamma S^\delta \quad (\text{Eq.3})$$

where P_m is the measured total monthly rainfall (mm) reported in the Lv11 database, E is the reported elevation (m) and S is a dummy variable to account for seasonality (S equals 1 for

the dry season, i.e. the months June to August, and 2 for the wet season). We used Lv11 data to train the model. A cross-validation procedure was used to assess the robustness of equation (3). We used 100 different and randomly selected calibration and validation datasets where 70% of the data was used for calibration and 30% for validation. We report the regression parameter median and ranges as well as indicators of model performance (Nash Sutcliffe model efficiency, root mean square error (RMSE) and R^2). We then used the 100 different calibration models to predict a distribution of 100 rainfall erosivities for each individual month using the observed monthly rainfall data from the Lv12 dataset ($R_m\text{.Lv12}$) (Figure 3).

2.4 Environmental covariates

Spatially continuous environmental covariates were used in both mapping procedures tested in this study (see Section 2.5) based on their known or potential influence on rainfall or rainfall erosivity patterns. After downloading the environmental covariates, bilinear interpolation was applied to the original layers in order to create homogeneous 1-km resolution layers. The environmental covariates considered in this study and their original sources are: (a) Monthly mean precipitation derived from the WorldClim database (Fick and Hijmans, 2017) reported for the period 1970 – 2000 at 30 arcsec resolution; (b) Monthly NDVI (normalized difference vegetation index) layers at 1-km resolution for the year 2017 derived from MODIS. Data were downloaded from the NASA website (lpdaac.usgs.gov/products/mod13a2v006), as the vegetation density affects evapotranspiration and rainfall intensities that are susceptible to rainfall erosivity; (c) Elevation from the 90 m resolution Digital Elevation Model (DEM) from Shuttle Radar Topography Mission (SRTM) of NASA (Jarvis et al., 2008). At the regional scale, precipitation varies strongly with elevation (Barry and

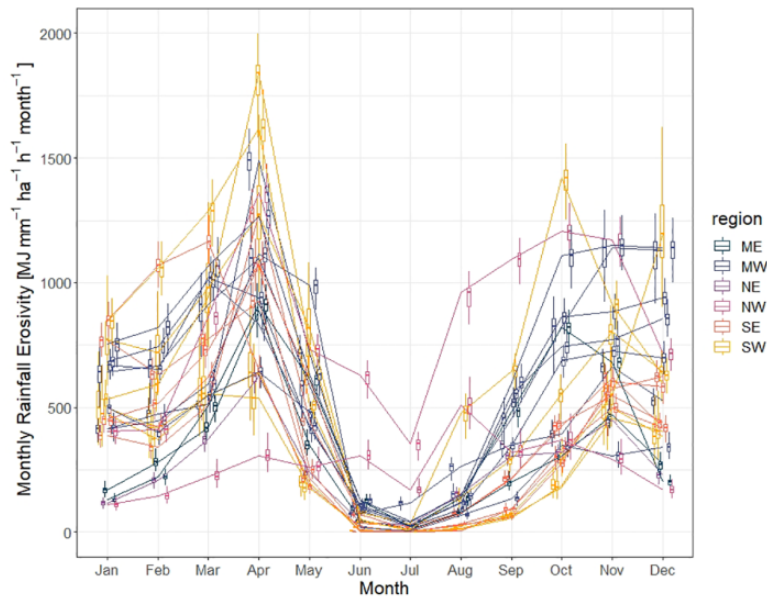


Figure 3. Predicted monthly Rm.Lvl2 based on the Lvl2 dataset using the 100 different parameter estimates from equation (3). The boxplots represent Rm.Lvl2 distribution from the 100 different model estimates. The color scale corresponds to the six regions defined in Figure 1.

Chorley, 2009) as relief features can induce different precipitation-elevation gradients depending partially on their ability to block and uplift moisture-bearing air (Daly et al., 2002). At the local scale, different climate regimes can occur depending on the orientation relative to air currents at larger scales (i.e. lee-ward and windward sides of mountains) and solar radiation. Hence, areas located at similar elevations may have different precipitation intensities. To address this, the 90 m resolution DEM was smoothed to two wavelengths of 5 and 20 km with a Gaussian filter. Slope and aspect layers were derived from the 20-km wavelength smoothed DEM to account for potential impact of large relief features (i.e. mountains range), and their main orientation toward moisture-bearing air. Then, eastness and northness were derived from the 5-km wavelength smoothed DEM to represent the degree to which hillslope aspect is close to the east and the north at smaller scale. Eastness and

northness were computed following the description in Zar (2010).

2.5 Spatial models of monthly and annual rainfall erosivity

Two different approaches (Nonlinear Least Square and Generalized Additive Models) were used and evaluated to model the spatial variability of both monthly and annual rainfall erosivity. Both approaches are environmental regressions supported by spatially continuous covariates that cover the LKR (see Section 2.4).

2.5.1 Nonlinear Least Square Model (NLS). The first approach, called the *NLS model*, is based on the direct application of equation (3) using spatially continuous environmental covariates instead of raw observed data. Hence, the 1-km resolution layers derived from the WorldClim 2.0 maps for the 1970–2000 period and the SRTM topography were used to estimate P , E

and S to be used in the model (equation (3)). We used the 100 different model parameter estimates for equation (3), as informed by the cross-validation procedure described above, to construct 100 monthly and annual rainfall erosivity maps. Based on these 100 spatial estimations, we computed the mean and the upper (Q_{95}) and lower (Q_5) percentiles for each pixel. The resulting mean prediction was used to map rainfall erosivity for the entire LKR, whereas the uncertainty was estimated as the difference between the Q_{95} and the Q_5 percentiles. The advantage of this approach is that it is directly informed by the analysis of the high temporal resolution Lvl1 dataset. However, the factors controlling rainfall erosivity, which are used as spatially continuous model inputs, are derived from global scale products, which may not fully capture the local spatial variability (particularly rainfall patterns).

2.5.2 Generalized Additive Models (GAM). The second approach is an environmental regression technique called *GAM* (Hastie and Tibshirani, 1986), and we applied it to the relationships between $Rm.Lvl2$ and the environmental covariates described above. This approach was used to produce 13 models: one per month and one annually. The GAM approach is a generalization of linear regression models (GLM) in which the coefficients are a set of smoothing functions, accounting for the non-linearity that could exist between the dependent variable (Y) and the covariates (X). As for GLMs, GAMs specify a distribution for the conditional mean $\mu(Y)$ along with a link function g relating the latter to an additive function of the covariates (equation (4)):

$$g[\mu(Y)] = a + f_1 x_1 + f_2 x_2 + \dots + f_p x_p \quad (\text{Eq.4})$$

where Y is the dependent variable, x_1, x_2, \dots, x_p represent the covariates and f_i 's are the smooth (non-parametric) functions and a constant.

For each monthly and aggregated annual time step, a model linking spatial variability of

rainfall erosivity to the most significant covariates was fitted. A Gaussian distribution model incorporated the conditional mean $\mu(Y)$ and a log-linear link function $g(\mu) = \log(\mu)$ was implemented. The smoothing functions of the models were built using regression splines, and the smoothing parameters were estimated by penalized Maximum Likelihood to avoid an over-fitting (Wood, 2001). An extra penalty added to each smoothing term allowed each of them to be set to zero during the fitting process in case of multi-collinearity or multi-concurvity. The spatial coordinates of the stations were added explicitly in each model as a two-dimensional spline on latitude and longitude in order to account for the spatial dependence and trends of the target variable at the regional scale. First, a model including all the covariates was fitted, which included precipitation, elevation, slope, aspect, eastness, northness and NDVI. Then, the covariates with a p -value > 0.05 were dropped, and the model refitted. To finish, a leave-one-out cross-validation procedure was applied, and coefficient of determination (R^2) and RMSE were calculated to quantify their goodness of fit. The mean model fitted as described above was successively readjusted to the corresponding 100 estimated $Rm.Lvl2$ sub-sets to produce 100 independent representations of the monthly and annual rainfall erosivity all over the study area. Based on these 100 spatial estimations, we computed the median, Q_{95} and Q_5 for each pixel. The resulting mean prediction was used to map rainfall erosivity for the entire LKR, whereas the uncertainty was estimated as the difference between the Q_{95} and the Q_5 percentiles. The GAM models have the advantage that they are directly fitted on measured monthly and annual rainfall patterns (i.e. the 24 Lvl2 stations) to give insights on the environmental covariates driving the spatial distribution of rainfall erosivity for each period of interest. However, the full potential of the GAM approach was not reached due to the relatively small number of Lvl2 stations.

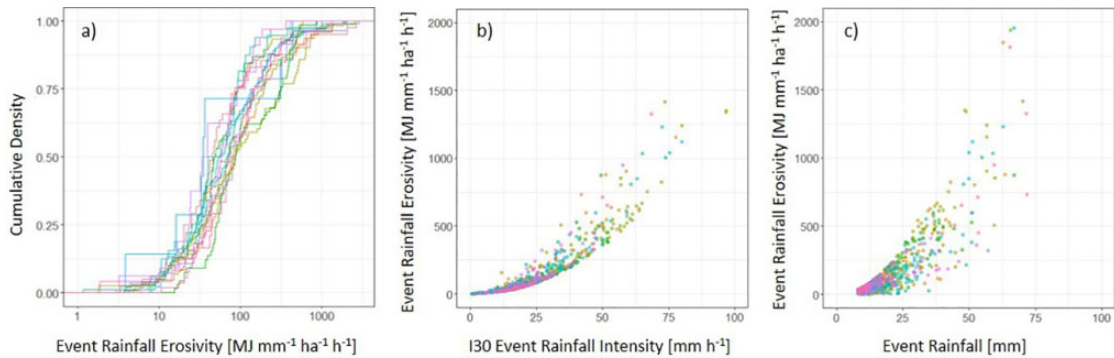


Figure 4. Rainfall erosivity of single events based on the TAHMO-5-min dataset. Cumulative distribution (a) and relationships between the rainfall erosivity and maximum 30-minute rainfall intensity (I30) (b) and rainfall amount (c). Colors show values of individual stations.

2.5.3 Comparison with existing large-scale estimations. Other studies have provided estimates of rainfall erosivity for the LKR, and these assessments are typically informed by coarser-scale observations as they target much larger spatial scales (continental or even global). Here, we evaluate the similarities and differences with our approach based on local and high-resolution observations in combination with spatial predictive models. We evaluate three models, presented by Vrieling et al. (2010), Karagame et al. (2016) and Panagos et al. (2017). We interpolated these three models to a 1-km grid resolution using a bilinear interpolation to facilitate a comparison with our predictions to consider the central area of the study region, which had a dense cover of Lvl1 stations. In the study of Karagame et al. (2016), they used the equation of Lo et al. (1985) to predict rainfall erosivity in the Lake Kivu basin (see Figure 7); however, this equation only accounts for the mean annual precipitation based on observations from Hawaii. Panagos et al. (2017) used a global dataset of long-term high-resolution rainfall data using sub-hourly and hourly pluviographic records for the 1950–2015 period (GREM model). The TRMM Multi-satellite Precipitation Analysis (TMPA) Model (Vrieling et al., 2010) examined

erosivity for Africa using 3-hourly and monthly TMPA precipitation data products for the period 1998–2008 at a 0.25° spatial resolution.

III Results

3.1 Data quality of the Lvl1 dataset

Out of the 445 station-months for which observations were available, 71% fulfilled the first data quality criteria stipulating that during more than 95% of the time data should be recorded. The resulting data set covers 315 station-months, equivalent to more than 26 observation years. A second quality assessment was based on the erosivity density, aggregated at a monthly time-scale. This analysis showed that a small number of meteorological stations were characterized by an exceptionally low erosivity density, although they received a similar amount of rainfall as nearby stations. An analysis of the distribution of erosivity densities per station (Figure S2) shows that four stations have a very low inter-quartile range with median erosivity density values below $0.5 \text{ MJ ha}^{-1} \text{ h}^{-1}$. Published observations on monthly erosivity densities for the region (Ryumugabe and Berding, 1992) show that these typically range between 1 and $5.5 \text{ MJ mm ha}^{-1} \text{ h}^{-1}$. We interpreted the much smaller ranges and absolute values for these four stations

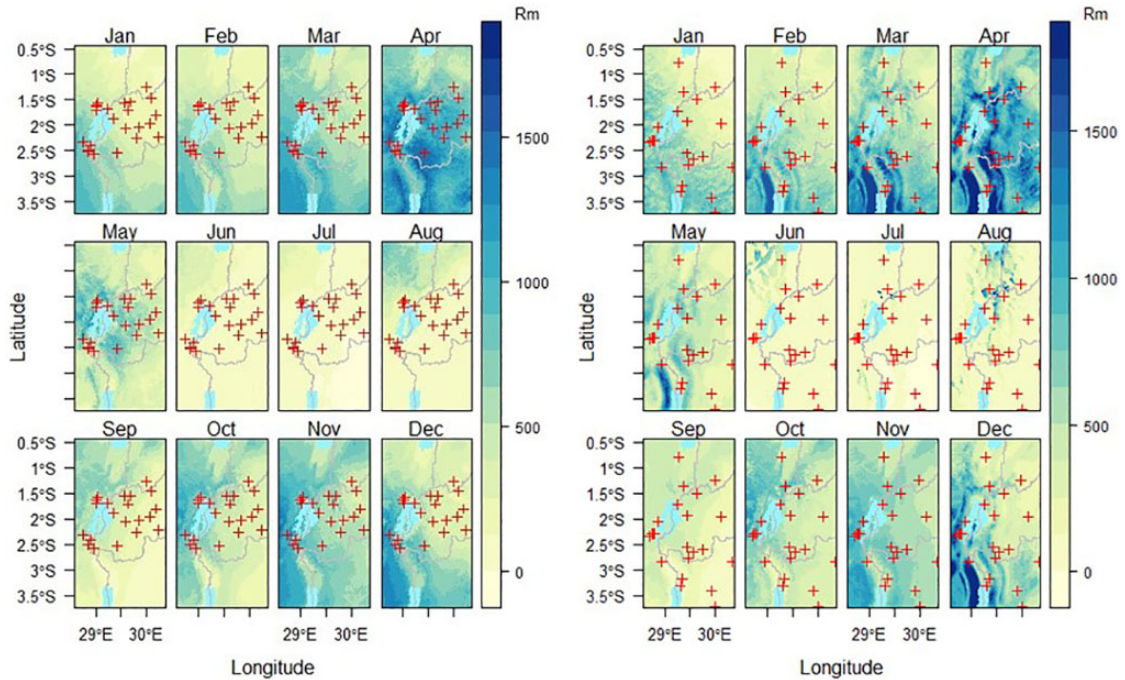


Figure 5. Mean monthly erosivity (1970-2000) based on the NLS (left) and the GAM (right) model. The crosses indicate the location of the Lv11 (for NLS) and the Lv2 (for GAM) meteorological stations.

as biased observations, most likely due to poor maintenance where the rainfall collector was clogged, which resulted in a large underestimation of rainfall intensities, but not rainfall amounts. We therefore excluded these four meteorological stations, representing 47 station-months, from the Lv11 database. In the analysis reported below, 268 station-months were used.

3.2 Event-scale erosivity

During the observation period, 918 erosive events were identified in the Lv11 dataset (Figure 4). All stations showed a similar distribution of rainfall erosivities per event with an average event erosivity of $194 \text{ MJ mm ha}^{-1} \text{ h}^{-1}$. The distributions are right-skewed where ca. 7% of the erosive events have an erosivity above $500 \text{ MJ mm ha}^{-1} \text{ h}^{-1}$. When considering all the stations, 6% of the most erosive events contributed

to 50% of the total erosivity and 3% of the erosive events had an erosivity $>1000 \text{ MJ mm ha}^{-1} \text{ h}^{-1}$. This shows that a few extreme events have a disproportionately high contribution to the total rainfall erosivity. The main factor controlling the event erosivity is the maximum rainfall intensity (I30), while the rainfall amount is less important (Figure 4 (b) and (c)).

We analyzed the effect of the temporal resolution of the data acquisition on the estimation of rainfall erosivity. When aggregating the original 5-minute rainfall data to 10, 30 and 60 minutes, we observed that rainfall data with a 10-minute resolution provided similar estimates of daily rainfall erosivity to that obtained with 5-minute interval data (Figure S1). However, a substantial underestimation of rainfall erosivity occurs when using data at 30 minutes (ca. 15% underestimation) and especially 60 minutes (ca. 46% underestimation). This is

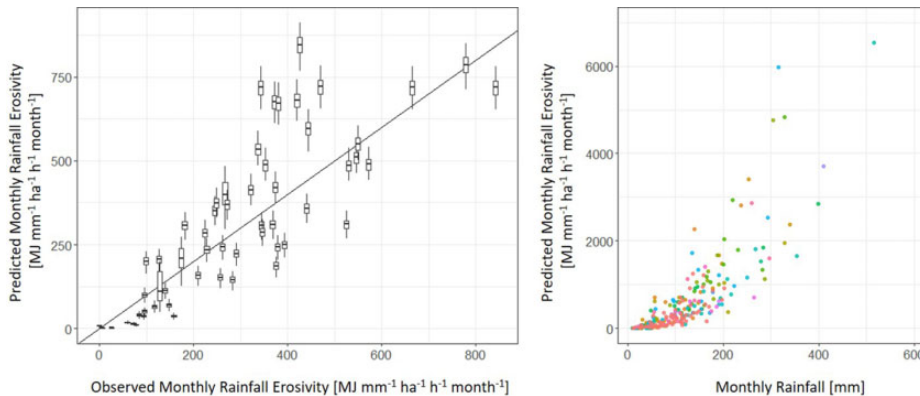


Figure 6. Left: External validation of Equation 3 using the data presented in Ryumugabe and Berding (1992). The boxplots represent the prediction uncertainty as derived from the 100 different parameter sets for equation (3). Right: Monthly EI₃₀ versus monthly precipitation for the Lvl1 dataset. Different colors indicate different meteorological stations.

related to the fact that the maximum rainfall intensity is substantially underestimated when using longer observation intervals. This analysis shows that high-resolution rainfall records, i.e. 10 minutes or less, are required to accurately estimate rainfall erosivity. However, the high predictive power of the regression models suggests that correction factors can be applied when using low temporal resolution data. For the Lvl1 dataset, we applied a correction factor of 1.15 (due to the 15% underestimation shown in Figure S1 middle panel) to the EI₃₀ estimates derived from Goma-OVG rainfall data (temporal resolution of 30 minutes) and added the Goma-OVG dataset to the Lvl1 database.

3.3 Monthly rainfall erosivity

For the 268 station-months observations of Lvl1, we could not detect a significant effect of latitude or longitude on R_m .Lvl1. Using equation (3) to predict trends in monthly erosivity, we obtained a median nash-sutcliffe efficiency (NSE) and RMSE of 0.75 and 459, respectively, with an interquartile range of 0.74–0.77 and 448–471. The regression coefficients of equation (3) were well constrained with median parameter estimates for α , β , γ and δ of 4.947, 1.895,

–0.5789 and –0.6808, respectively. The negative values for β and γ imply that for the same amount of monthly rainfall, erosivity is higher at lower altitudes and during the dry season.

The 100 different monthly rainfall- R_m models (equation (3)) were then applied to the Lvl2 dataset to estimate the variability of the monthly erosivity in the study region (Figure 3). The estimated monthly rainfall erosivity for the Lvl2 stations ranged between 0 and 2000 MJ mm^{–1} ha^{–1} h^{–1} month^{–1}. The regional variability is high, with an average monthly coefficient of variation of ca. 50% for the wet season. It should be noted that the uncertainty associated with the predictions, as estimated from the cross-validation, is much smaller than the regional and seasonal variability. As expected, the erosivity follows the general rainfall patterns with a pronounced period with low erosivity, i.e. from June to August. The cumulative annual erosivity for the Lvl2 stations ranges between ca. 3000 and 9000 MJ mm^{–1} ha^{–1} h^{–1} yr^{–1} with a mean of ca. 5683 MJ mm^{–1} ha^{–1} h^{–1} yr^{–1} (Table S2).

3.4 Spatial patterns of rainfall erosivity

3.4.1 NLS model. The rainfall erosivity follows the north–south translocation of the thermal

Table 1. Parameters related to the calibration and validation procedure of the generalized additive models (GAM) predicting the annual and monthly rainfall erosivity (Rm) in the Lake Kivu region. R^2 is the coefficient of determination and RMSE the root mean square error obtained from the LOOCV procedure (Leave-One Out Cross-Validation).

	Calibration Variance explained (%)	Validation (LOOCV)	
		R^2	RMSE (MJ mm ha ⁻¹ h ⁻¹ month ⁻¹)
Year	88	0.65	1122
January	92	0.71	135
February	91	0.7	147
March	96	0.86	139
April	77	0.38	355
May	74	0.48	167
June	90	0.82	41
July	90	0.23	42
August	95	0.24	226
September	81	0.54	128
October	93	0.61	179
November	61	0.44	178
December	93	0.61	191

equator during the wet seasons (Figure 5). In general, the highest values of rainfall erosivity are found in the highland part of the LKR and surrounding Lake Kivu (Figure 5). In April, the highlands of the eastern part are the most erosive, while in November and December erosivity migrates to the western highlands. These east–west erosive movements are driven by the seasonal rainfall patterns. The annual rainfall erosivity in the region ranges between 2000 and 9000 MJ mm⁻¹ ha⁻¹ h⁻¹ yr⁻¹ and has a pronounced east–west gradient, where the highest values occur in the East. This is mainly controlled by local topography. In the central part, erosivity is lower due to the lower altitudes near the lakes. The uncertainty, as estimated from the interquantile range of the 100 model scenarios, follows the same pattern as the annual erosivity, with an average relative error of ca. 20 to 35%.

3.4.2GAM model. Table 1 presents parameters describing the goodness of fit of the 13 GAM models. The amount of variance explained by the models during the calibration procedure

Table 2. Significance level of the environmental covariates selected in the final generalized additive models (GAM) predicting annual R and monthly (Rm) rainfall erosivity in the Lake Kivu region.

Month	Precipitation	Elevation	Slope	Aspect	Eastness	Northness	NDVI
January	***	*	***	-	-	-	-
February	***	***	**	-	-	-	**
March	***	***	***	-	-	*	-
April	***	-	***	*	-	-	-
May	***	-	***	-	-	-	-
June	-	-	-	-	***	*	-
July	-	***	-	-	*	-	**
August	-	*	*	-	**	***	*
September	***	-	-	-	-	-	-
October	***	**	-	-	-	-	**
November	***	-	-	-	-	-	-
December	***	*	***	**	-	-	-
Year	***	-	***	-	-	*	-

NDVI: normalized difference vegetation index.

varied from 61% for November to 93% for December, and equaled 88% for the annual data. While the validation procedure produced R^2 between 0.44 and 0.86 for most of the monthly models, two of the driest months (July and August) showed much lower R^2 of 0.23 and 0.24, and the wettest month April a R^2 of 0.38. It should be noted that the dataset of 24 stations is relatively small and that there are not many stations in high-altitude areas (Figure 1). This influences a larger residue in the LOOCV (Leave-One Out Cross-Validation) procedure and leads to a lower R^2 , particularly for months with low erosivity (Table 1). The GAM model at the annual timescale showed a good performance with an R^2 of 0.65 and an RMSE of $1122 \text{ MJ mm}^{-1} \text{ ha}^{-1} \text{ h}^{-1} \text{ yr}^{-1}$ during the validation.

Table 2 presents the environmental covariates kept in each final model after the calibration procedure. As expected, the mean monthly precipitation was selected as one of the most influential covariates explaining R_m variability. Indeed, it was selected to spatialize R_m for the whole year and for 9 of the 12 months which covered the period from September to May, which included the rainy season for southern stations and both rainy seasons for center and northern stations (Figure 1). The slope, derived from the 20-km wavelength filtered DEM, was also selected in the final models for six of the nine wettest months cited above (particularly during the most erosive months) highlighting the influence of large relief features on rainfall erosivity in the LKR. For the months June to August (including the dry season occurring all over the study area), the mean precipitation was not selected, but elevation and/or eastness and northness appeared as important covariates here. Hence, spatial variability of erosivity during the dry season was influenced by local morphology. GAM models developed for June, July and August showed that hillslopes subject to highest erosivity were mainly oriented SE, E and NE. However, it should be noted that as explained by Laceby et al. (2016),

the inconsistent selection of some covariates in the GAM models does not signify that they do not influence rainfall erosivity, as the covariates could not have been retained in the final model if there are multi-collinearity or concavity between covariates. Therefore, the non-selection of covariates can mean that other covariates likely have a similar, though stronger, mathematical relationship with the target variable.

Erosivity predictions based on the GAM model show, overall, that the spatial and temporal trends are consistent with those derived from the NLS model, although the GAM predictions show more spatial variability, particularly in regions with steep topography and lowlands. This is also shown in the uncertainty maps, as reflected by the Q_{05} – Q_5 range (Figure S3).

IV Discussion

Rainfall erosivity studies are inherently confronted with a tradeoff between high-resolution temporal and spatial rainfall erosivity data. This is particularly the case for data-poor regions such as the Lake Kivu region. In this study, we evaluated to what extent the combination of high temporal resolution data (but with poor spatial and long-term coverage) and low temporal resolution (but high spatial density covering long periods of time) data can address this issue. In the following section, we discuss the potential and limitations of the two different approaches adopted in this study and confront our estimates with existing studies.

4.1 Erosivity estimation

Although the TAHMO observations were very informative for rainfall erosivity assessments, we observed issues with data gaps, and most stations only provide data for a relatively short period of time. Our data analysis clearly demonstrated that high temporal resolution (<10 minutes) data is critical to correctly estimate rainfall erosivity. At coarser resolutions (30 or 60 minutes) maximum rainfall intensities become

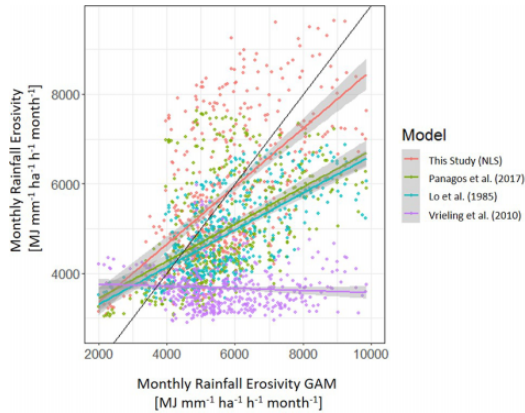


Figure 7. Comparison of the GAM model with existing estimates from the literature.

substantially underestimated. The underestimation of the rainfall erosivity when using hourly data (ca. 50%) is consistent with those reported by other studies from Europe (Panagos et al., 2015) and globally (Panagos et al., 2017). Furthermore, we demonstrated that high temporal resolution data can be used to develop models that relate monthly total rainfall with estimates of erosivity. We found that monthly erosivity estimators (R_m) exploiting monthly rainfall data (P_m) in a power model relationship described the observed erosivity relatively well, consistent with findings of other studies (Karame et al., 2016). However, we observed that rainfall erosivity was not only controlled by precipitation, but that elevation and season are also significant controls, and these factors were therefore included in the prediction model. The results of a cross-validation to predict monthly rainfall erosivity show that the prediction models are robust. An external validation was performed using monthly rainfall erosivity estimates for four stations in Rwanda (Ryumugabe and Berding, 1992) (Figure 6). The external validation, with an RSME of $136 \text{ MJ mm ha}^{-1} \text{ h}^{-1} \text{ month}^{-1}$ and a NSE of 0.67, shows that our monthly model based on rainfall, elevation and season is capable of describing the regional trends relatively well,

but that substantial uncertainties remain associated with point predictions. However, it should be noted that the stations used by Ryumugabe and Berding (1992) are located at low altitudes and have a low erosivity, relative to the stations used in this study (Lv11 dataset).

4.2 Spatial and temporal patterns of erosivity

We tested two approaches to model the spatio-temporal variability of rainfall erosivity in the region. The first approach consisted of applying the NLS model (equation (3); developed on the Lv11 dataset) using spatially explicit global datasets that estimate elevation and long-term monthly rainfall. The predictions therefore largely depend on the quality of the spatial input data, which are both global data products. We also used an alternative approach where rainfall erosivity was first estimated at points for which high-quality long-term monthly rainfall was available and which has a good spatial regional coverage (Lv12 dataset) compared to the Lv11 dataset. An environmental regression approach (GAM) was then applied to assess the seasonality and spatial patterns. The overall patterns of monthly erosivity were similar for the two approaches (Figure 5), with the GAM putting more emphasis on topographical features considering different spatial scales (mountain ranges and local hillslopes). The GAM predictions show, however, much more spatial variability at short scales due to the inclusion of more environmental covariates. The LKR shows highest erosivity values in the months March and April, and November and December (Figure 5). The highest mean rainfall erosivity is observed in April, while the lowest mean rainfall erosivity occurs in the middle of the dry season in July (Figure 5). In general, rainfall erosivity follows the thermal equator and the ITCZ, while at a more local scale the highest values of rainfall erosivity are found in the highlands. The average regional annual erosivities

derived from the NLS and GAM modeling for the study region are similar with a mean of 5482 and 5523 MJ mm ha⁻¹ h⁻¹ yr⁻¹, respectively. Lower values are observed for the eastern part of the region and at lower altitudes. The maximum values predicted for the region are found in the western highlands (ca. 10,000 MJ mm ha⁻¹ h⁻¹ yr⁻¹), and are consistent with estimates from other tropical mountain areas. For example, Goç Alves et al. (2006) and Montebeller et al. (2007) found mean values of between 10,000 and 12,000 MJ mm ha⁻¹ h⁻¹ yr⁻¹ for the Mountainous Region of Rio de Janeiro state.

4.3 Prediction uncertainties

We explicitly assessed the uncertainties associated with the estimation of rainfall erosivity. Using the Q₅–Q₉₅ percentile range of the 100 model simulations for both the NLS and GAM models, we obtained mean relative errors in the order of 20 to 35% for the study region, where the uncertainty was highest in the highlands and lowlands areas near Lake Tanganyika and Lake Edward. However, the GAM model resulted locally in higher uncertainties in regions where no observations were present to constrain the spatial model. The uncertainty of the spatial predicted values are a combination of the uncertainties associated with the estimation of Rm.Lvl1 and Rm.Lvl2, i.e. the erosivity at the meteorological stations, and the approximation of the controlling variables by a set of simplified covariates. Although at present the field-based data to corroborate our two spatial model approaches are not available, we suggest that the GAM model has more predictive power as it relies on regional data for both EI₃₀ calculations and measured spatial patterns of monthly rainfall. The NLS model required usage of a global product for the estimation of rainfall patterns. The quality of the spatial models will substantially benefit from more data, i.e. from a denser network of stations covering longer periods of time, particularly in the highlands where

uncertainties are highest. With respect to the length of the data series, it is generally accepted that a minimum of 20 years is desirable for rainfall erosivity analysis (Curse et al., 2006; Verstraeten et al., 2006) without data gaps. It should be noted that we used long-term averages and did not capture changes in rainfall erosivity due to climate change or decadal trends. At present, the required data to do so is not available. TAHMO network has the potential to continuously increase the performance of spatial prediction models and to assess temporal changes as well. The spatial model approaches developed here have the potential to improve the quantification of rainfall erosivity in Africa, but this will require the expansion of the database where more stations will have long-term rainfall records.

4.4 Comparison with existing large-scale estimates

Comparison with other published estimates shows that there are substantial differences particularly with the coarse-scale Vrieling et al. (2010) model, which substantially underestimates rainfall erosivity by ca. 40% relative to our estimates (Figure S4). The other two approaches have spatial patterns which are more consistent with our approach, as they use similar environmental covariates. Nevertheless, there is substantial scatter, and the R² between the GAM model and the GREa model is only 0.25 (Figure 7). There is also a consistent bias with an under prediction of about 20 to 25% of the annual rainfall erosivity, when compared to our approach. The underestimation occurs mostly at higher rainfall erosivities. This shows that the regions with higher rainfall erosivities, particularly in the highlands, are not well represented in existing estimates.

V Conclusion

For a better understanding of the spatial and temporal variability of rainfall erosivity in the understudied region of the LKR we used freely

available geospatial datasets. Despite some limitations (limited observation period, limited spatial coverage) in the datasets, several conclusions can be drawn:

1. *Using data from the Trans-African Hydro-Meteorological Observatory for the period 2017–2020*, we analyzed rainfall erosivity for 20 meteorological stations in the LKR and found that rainfall amount, elevation and season were the main factors controlling rainfall erosivity. Based on an observational database covering more than 260 station-months in the LKR, equivalent to more than 22 observation years, we developed a predictive model that had a modeling efficiency of 75%.
2. *By combining high and low temporal resolution databases*, we developed monthly and annual spatial prediction models to provide regional assessments based on locally calibrated and validated data. This approach addresses the tradeoff between spatial and temporal resolution and limitations related to short observation periods and can serve as a template for other regions and can be continuously improved when more data becomes available.
3. *Existing approaches* are able to represent, to some extent, the general spatial patterns of rainfall erosivity in the Lake Kivu region, but consistently underestimate rainfall erosivity, particularly in the highlands.
4. *Community-based meteorological observatories* can be used to substantially improve the spatial and temporal assessment of rainfall erosivity in data-poor regions. This requires a careful consideration of data quality and methods to address the occurrence of data gaps.


Declaration of conflicting interests

The author(s) declared no potential conflicts of interest with respect to the research, authorship, and/or publication of this article.

Funding

The author(s) disclosed receipt of the following financial support for the research, authorship, and/or publication of this article: This study was conducted under the research project “Human impact on flux sediments in the Lake Kivu region” funded by the Université Catholique de Louvain (UCL), Goma Volcano Observatory (OVG), the World Bank and the Fonds de la Recherche Scientifique FNRS (project numbers T.0059.18 and J.0167.19).

ORCID iD

S. Baumgartner  <https://orcid.org/0000-0002-4091-9164>

Supplemental material

Supplemental material for this article is available online.

References

- Adetan O and Afullo TJ (2014) Raindrop size distribution and rainfall attenuation modelling in equatorial and subtropical Africa: The critical diameters. *Annals of Telecommunication* 69: 607–619.
- Angima S, Stott D, O'Neill M, et al. (2003) Soil erosion prediction using RUSLE for central Kenyan highland conditions. *Agriculture, Ecosystems & Environment* 97: 295–308.
- Arnoldus H (1977) Methodology used to determine the maximum potential average annual soil loss due to sheet and rill erosion in Morocco. *FAO Soils Bulletins* 34: 8–9.
- Ballesteros AL, Beck J, Bombelli A, et al. (2018) Towards a feasible and representative pan-African research infrastructure network for GHG observation. *Environmental Research Letters* 13: 085003.
- Barry RG and Chorley RJ (2009) *Atmosphere, Weather and Climate*. London, UK: Routledge, 636.
- Bonilla CA and Vidal KL (2011) Rainfall erosivity in Central Chile. *Journal of Hydrology* 410: 126–133.
- Brown LC and Foster GR (1987) Storm erosivity using idealized intensity distributions. *Transactions of the ASAE* 30: 379–386.
- Courtois AC and Manirakiza R (2015) La repartition de la population. In: *Atlas des pays du Nord-Tanganyika*. Marseille: IRD Editions, 52–55.
- CROPWAT Software, FAO (2018) Land and water division. Available at: <http://www.fao.org/land-water/data-bases-and-software/cropwat/>

- Curse R, Flanagan J, Frankenberger B, et al. (2006) Daily estimates of rainfall, water runoff and soil erosion in Iowa. *Journal of Soil and Water Conservation* 61: 191–199.
- Daly C, Gibson WP, Taylor GH, et al. (2002) A knowledge based approach to the statistical mapping of climate. *Climate Research* 22: 99–113.
- Elagib N (2011) Changing rainfall, seasonality and erosivity in the hyperarid zone of Sudan. *Land Degradation & Development* 22: 505–512.
- Fick SE and Hijmans RJ (2017) Worldclim 2: New 1 km spatial resolution climate surfaces for global land areas. *International Journal of Climatology* 37: 4302–4315.
- Goçalves FA, Silva DD, Pruski FF, et al. (2006) Índices e espacialização da erosividade das chuvas para o Estado do Rio de Janeiro. *Revista Brasileira de Engenharia Agrícola e Ambiental* 10: 269–276.
- Hastie T and Tibshirani R (1986) Generalized additive models. *Statistical Science* 1: 297–310.
- Igwe C, Mbagwu J and Akamigbo F (1999) Application of SLEMSA and USLE models for potential erosion hazard mapping in southeastern Nigeria. *International Agrophysics* 13: 41–48.
- Ilunga L, Mbaragijimana C and Muhire I (2004) Pluviometric seasons and rainfall origin in Rwanda. *Geo-Eco-Trop* 28: 61–68.
- Jarvis A, Reuter HI, Nelson A, et al. (2008) Hole-filled SRTM for the globe Version 4, available from the CGIAR-CSI SRTM 90 m Database. Available at: <http://srtm.csi.cgiar.org>
- Karagame F, Hua Shao F, Xi C, et al. (2016) Deforestation effects on soil erosion in the Lake Kivu Basin, D.R. Congo-Rwanda. *Forest* 7: 281.
- Laceyby JP, Chartin C, Evrard O, et al. (2016) Rainfall erosivity in catchments contaminated with fallout from the Fukushima Daiichi nuclear power plant accident. *Hydrology and Earth System Sciences* 20: 2467–2482.
- Le Roux J, Morgenthal T, Malherbe J, et al. (2008) Water erosion prediction at a national scale for South Africa. *Water SA* 34: 305–314.
- Lo A, El-Swaify SA, Dangler EW, et al. (1985) Effectiveness of EI30 as an erosivity index in Hawaii. In: El-Swaify SA and Moldenhauer WC (eds) *Soil Erosion and Conservation*. Ankeny: Soil Conservation Society of America, 384–392.
- McGregor KC, Bingner RL, Bowie AJ, et al. (1995) Erosivity index values for northern Mississippi. *Transactions of the ASAE* 38: 1039–1047.
- Montebeller CA, Ceddia MB, Carvalho DF, et al. (2007) Variabilidade espacial do potencial erosivo das chuvas no Estado do Rio de Janeiro. *Engenharia Agrícola* 27: 426–435.
- Muhire I, Ahmed F and Abd Elbasit MMM (2015) Spatio-temporal variations of rainfall erosivity in Rwanda. *Academic Journals* 6: 72–83.
- Ndayirukiye S and Sabushimike JM (2015) Les climats et les mécanismes climatiques. In: *Atlas des pays du Nord-Tanganyika*. Marseille: IRD Editions, 28–31.
- Panagos P, Borrelli P, Meusburger K, et al. (2015) Modelling the effect of support practices (P-factor) on the reduction of soil erosion by water at European scale. *Environmental Science & Policy* 51: 23–34.
- Panagos P, Borrelli P, Meusburger K, et al. (2017) Global rainfall erosivity assessment based on high-temporal resolution rainfall records. *Scientific Reports* 7: 4175.
- Renard KG and Freimund JR (1994) Using monthly precipitation data to estimate the R-factor in the revised USLE. *Journal of Hydrology* 157: 287–306.
- Roose E (1977) Erosion et ruissellement en Afrique de l'Ouest, vingt années de mesures en parcelles expérimentales. *O.R.S.T.R.O.M.* 78: 30–33.
- Rutebuka J, De Taeyea S, Kagaboc D, et al. (2020) Calibration and validation of rainfall erosivity estimators for application in Rwanda. *Catena* 19: 104538.
- Ryumugabe JB and Berding FR (1992) Variabilité de l'indice d'agressivité des pluies au Rwanda. In: *Réseau Erosion, Bulletin*. Montpellier: Centre ORSTOM de Montpellier, 113–119.
- Salako FK (2010) Development of erodent maps for Nigeria from daily rainfall amount. *Geoderma* 156: 372–378.
- Smithen A and Schulze R (1982) The spatial distribution in Southern Africa of rainfall erosivity for use in the universal soil loss equation. *Water SA* 8: 74–78.
- USDA (2019) *Agricultural Research Service. RIST - Rainfall intensity Summarization Tool*. United States: Department of Agriculture.
- Vantas K, Sidiropoulos E and Evangelides C (2019) Rainfall erosivity and its estimation: conventional and machine learning methods. In: Vlassios H and

- Konstantinos K (eds) *Soil Erosion – Rainfall Erosivity and Risk Assessment*. Rijeka: IntechOpen.
- Verstraeten G, Poesen J, Demarée G, et al. (2006) Long-term (105 years) variability in rain erosivity as derived from 10 min. rainfall depth data for Ukkel (Brussels, Belgium): Implications for assessing soil erosion rates. *Journal of Geophysical Research Atmospheres* 111: D22109.
- Vrieling A, Sterk G and Steven MDJ (2010) Satellite-based estimation of rainfall erosivity for Africa. *Journal of Hydrology* 395: 235–241.
- Wischmeier WH and Smith DD (1958) Rainfall energy and its relationship to soil loss. *Transactions American Geophysics Union* 39: 285–291.
- Wischmeier WH and Smith DD (1978) *Predicting Rainfall Erosion Losses: A Guide to Conservation Planning*. Agriculture Handbook 537. USA: USDA-ARS.
- Wood SN (2001) MgcV GAMs and generalized ridge regression for R. *R news* 1: 2–25.
- Zar JH (2010) *Biostatistical Analysis*, 5th edition. New Jersey: Prentice Hall.